Turkish Journal of Physics

Volume 29 | Number 3 Article 4

1-1-2005

Mössbauer, Infrared and X-ray Studies for Ni_{0.5}Zn_{0.5}Cr_xFe_{2-x}O_4 Ferrites

MOHAMED AMER

S. ATA-ALLAH

T. MEAZ

S. ABOUL-ENEIN

M. ABD-EL-HAMID

Turk J Phys
29 (2005) , 163 – 177.

Mössbauer, Infrared and X-ray Studies for $Ni_{0.5}Zn_{0.5}Cr_xFe_{2-x}O_4$ Ferrites

Mohamed AMER[1], Samy ATA-ALLAH[2], Talaat MEAZ[1], Saad ABOUL-ENEIN[1], Mohamed ABD-EL-HAMID[3]

[1] *Physics Department, Faculty of Science, Tanta University, Tanta, EGYPT*
e-mail: moazamer@yahoo.com
[2] *Reactor and Neutron physics Department, Nuclear Research Center, Atomic Energy Authority, Cairo, EGYPT*
[3] *Physics Department, Faculty of Science, Minia University, Minia, EGYPT*

Received 30.11.2004

Abstract

Spinel ferrites of the system $Ni_{0.5}Zn_{0.5}Cr_xFe_{2-x}O_4$, $0 \leq x \leq 1$, have been studied via Mössbauer, IR and X-ray spectra. Mössbauer spectra of the samples showed broad six-line patterns and a central paramagnetic phase. The spectra have been analyzed to two magnetic patterns, A and B, and two quadrupole doublets, C_A and C_B. The patterns A and C_A are assigned to Fe^{3+} ions at the tetrahedral A-sites and the patterns B and C_B to Fe^{3+} and Fe^{2+} ions at the octahedral B-sites. The deduced hyperfine interaction parameters; the isomer shifts, quadrupole splitting, outermost line widths, hyperfine magnetic fields and bulk magnetization were studied and discussed as functions of the Cr^{3+} additions x. The cation distribution of the compounds was estimated using the site preference of elements and the area ratio of B- to A-sites. The broad magnetic pattern B has been fitted to several subpatterns. Using the obtained hyperfine parameters one could assign each of the B-subpatterns to a component depends on the number of nonmagnetic Zn^{2+} ions as A-site nearest neighbours of the Fe ions at the B-sites. Five absorption bands were observed in the infrared spectra in the range between 1100 and 200 cm^{-1}. These bands are assigned to the Fe^{3+} ions on A-sites; to Fe^{3+} and Cr^{3+} ions on B-sites; to divalent ions Fe^{2+} and Ni^{2+} and to the energy of the lattices. The existence of Fe^2 ions on the A- and B-sites has been confirmed. From X-ray analysis, the average, true, and theoretical lattice parameters, the theoretical and bulk densities, the porosity, the oxygen parameter and the ionic radii, bonds, edges and hopping lengths of the A- and B-sites have been calculated and discussed depending on the Cr^{3+} ion content x. The dependency of the hyperfine field on the hopping length at the A- and B-sites has been studied and discussed.

Key Words: Mössbauer, Infrared, X-ray and ferrites.

1. Introduction

Spinel ferrites are still one of the basic materials of modern electronics and computer techniques. Ni-Zn ferrites are attractive for application in microwave and radio frequency devices owing to their high resistivity, mechanical hardness, and high Curie temperature and chemical stability. In earlier works, some authors [1–3], investigated the effect of some additives and substitutions on the physical properties of Ni-Zn

ferrites required for high frequency technique. It has been found that the main physical properties of spinel ferrites arise from the cationic distribution amongst the tetrahedral A- and octahedral B-sites [4, 5]. The parameters related to the ionic charge and radius, crystal fields play an important role in the site preference of the cations. The effect of Cr^{3+} substitution for Fe^{3+} in spinel ferrites [6–8] has been studied extensively. The results showed that Cr ions are in the charge state Cr^{3+} and intensively occupy the B-sites. When Cr^{3+} is progressively replaced by Fe^{3+} ions, the crystal structure becomes a cubic spinel structure and its Neel temperature rises. The addition of Cr^{3+} ions gives interesting Mössbauer and IR spectra and drastically changes the corresponding parameters. Consequently, the aim of the present work is to study the effect of Cr^{3+} substitution for Fe^{3+} on the physical properties of the spinel system $Ni_{0.5}Zn_{0.5}Cr_xFe_{2-x}O_4$, $0 \leq x \leq 1$. The techniques used in this study are the Mössbauer, infrared and X-ray diffraction spectrometers.

2. Experimental

The spinel samples of the system $Ni_{0.5}Zn_{0.5}Cr_xFe_{2-x}O_4$, $x = 0$, 0.2, 0.4, 0.6, 0.8 and 1, were prepared by the usual ceramic technology from the high purity oxides NiO, ZnO, Cr_2O_3 and Fe_2O_3. The sample powders were presintered at 1000 °C for one day. Finally the powder samples were pressed into pellets and sintered at 1200 °C for one day and quenched at room temperature. The X-ray diffraction patterns were taken using a Shimadzu X-ray diffractometer XD-3, where a copper X-ray source was used. The recorded reflection planes, as shown in Figure 1, are (220), (311), (222), (400), (422), (511), (440) and (622). Consequently, the appearance of these reflection planes proved that all the prepared samples have cubic spinel structure. The lattice parameter a,bulk density D,X-ray density D_x and porosity P were determined as indicated previously [9].

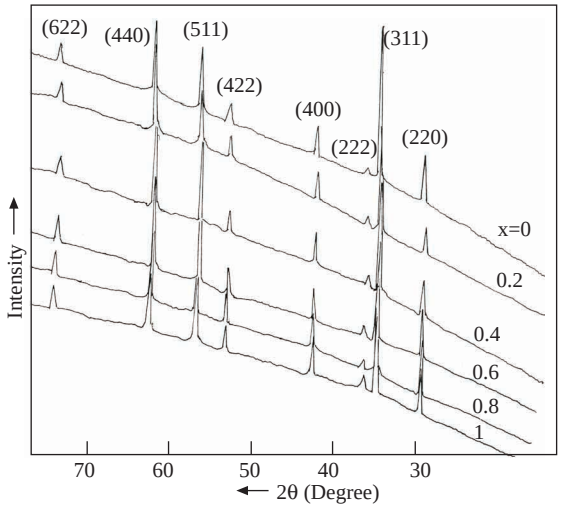

Figure 1. The X-ray diffraction patterns of the $Ni_{0.5}Zn_{0.5}Cr_xFe_{2-x}O_4$ ferrites.

Figure 2 shows the recorded Mössbauer spectra at room temperature. The Mössbauer spectrometer of the electromechanical type was used in the constant-acceleration mode. The source was ^{57}Co in Rh matrix at room temperature, where metallic iron was used for calibration. The spectra were analyzed using the least squares fit computer program. The spectra show a broadened Zeeman six-line pattern and a central paramagnetic phase C for all samples. However, two magnetic patterns A and B and two quadrupole doublets C_A and C_B could be identified in analyzing the spectra. The sharper magnetic pattern A and the doublet C_A were assigned to Fe^{3+} ions at the tetrahedral A-sites and the broadening pattern B and C_B to Fe^{3+} and Fe^{2+} at the octahedral B-sites. The broad magnetic pattern B in the spectra for $x \leq 0.8$ appeared to be composite. Consequently, the pattern B was fitted into several components B_n, $n = 0$, 1, 2, and 3, to

obtain the B-site subpatterns, as shown in Figure 2. The infrared absorption spectra were recorded at room temperature using the solid potassium bromide method. The spectra were taken employing a Perkin-Elmer 1430 spectrometer in the range from 4000 to 200 cm^{-1}.

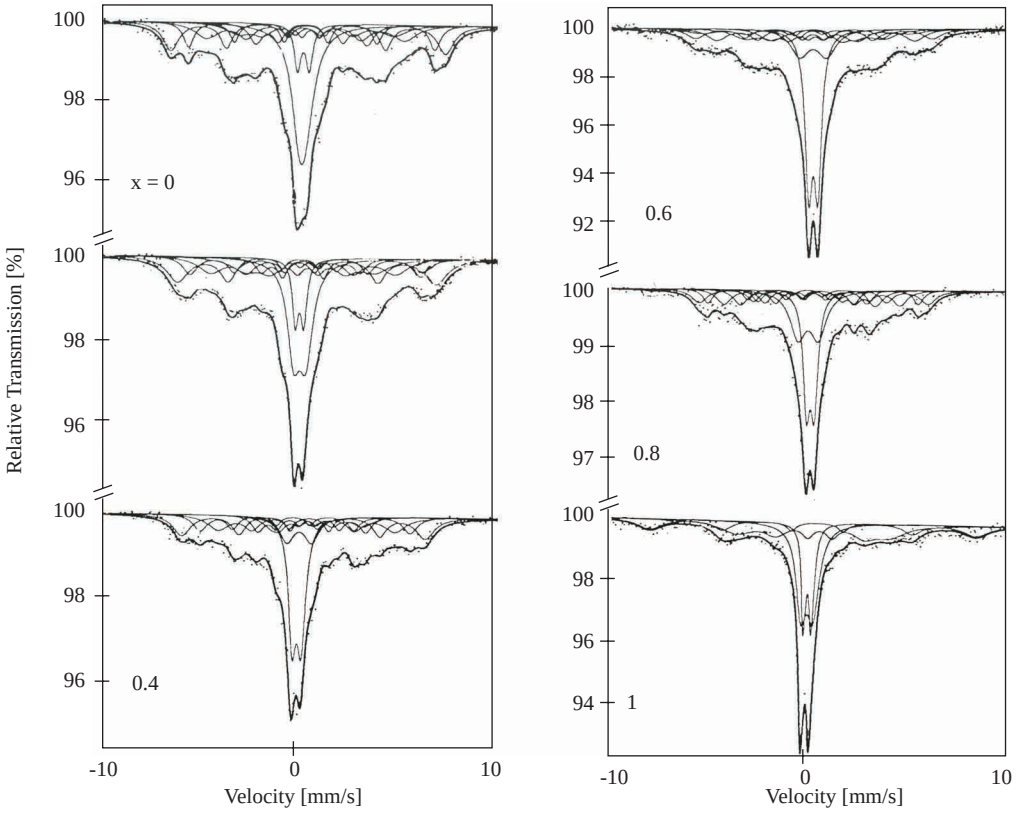

Figure 2. The Mössbauer spectra of the system $Ni_{0.5}Zn_{0.5}Cr_xFe_{2-x}O_4$. The solid lines through the data points are the results of the least-squares fit of sets of sextet and doublet patterns to the experimental data. The solid lines above the data points are the individual component lines.

3. Results and Discussion

3.1. Mössbauer spectra

Figure 2 shows the room temperature Mössbauer spectra of the $Ni_{0.5}Zn_{0.5}Cr_xFe_{2-x}O_4$ ferrites. The spectra show a broadened six-line pattern and a central paramagnetic phase C for all samples. This behavior is due to statistical fluctuations in the distribution of magnetic and nonmagnetic ions. The phase C arises from those Fe^{3+} ions, which are located within regions which are so small that they behave superparamagnetically [10, 11]. The broad magnetic pattern B in the spectra for $x \leq 0.8$ appeared to be composite because of the random distribution of the nonmagnetic Zn^{2+} ions among the A- and B-sites in addition to Fe^{3+} and Ni^{2+} ions. Hence, the octahedral B-site Fe^{3+} or Fe^{2+} may have nZn^{2+} ions, $n = 0, 1, \ldots, 6$, occupying its six nearest A-sites. The Fe ion carries the highest magnetic field and Zn^{2+} does not. Accordingly, the superexchange interaction between the B-site Fe ion and its six nearest neighbor A-cations depends on the population of Zn^{2+} ions among the six A-cations. In addition, the s-electron density at the nucleus of octahedral Fe cation is also likely to be dependent on the composition of the six tetrahedral nearest neighbors. Thus the pattern B must be composite and it has been analyzed to its subpatterns B_n, $0 \leq n \leq 3$. The obtained results from the fits are listed in Table 1.

Table 1. The Mössbauer parameters of the system $Ni_{0.5}Zn_{0.5}Cr_xFe_{2-x}O_4$, where H, ε_Q, δ, $\Gamma_{1,6}$ and A_o are the hyperfine magnetic field, quadrupole shift (or the quadrupole splitting), isomer shift, outermost line width and fractional area of each pattern, respectively.

X	Patterns	H (T)	ε_Q (mm/s)	δ (mm/s)	$\Gamma_{1,6}$(mm/s)	A_o
0	A	42.71	0.1	0.15	0.98	0.23
	B_0	38.3	0.29	0.27	0.7	0.09
	B_1	30.77	0.1	0.17	1.42	0.14
	B_2	24.15	0.43	0.34	1.55	0.13
	B_3	17.28	0.04	0.39	0.81	0.09
	C_A	—-	0.58	0.02	0.41	0.07
	C_B	—-	0.32	0.02	0.99	0.25
0.2	A	40.19	0.18	0.13	1.29	0.21
	B_0	35.9	0.23	0.15	0.89	0.1
	B_1	28.69	0.17	0.14	1.48	0.15
	B_2	20.05	0.12	0.4	1.73	0.15
	B_3	15.25	0.14	0.47	0.73	0.07
	C_A	—-	0.42	-0.01	0.46	0.08
	C_B	—-	0.61	0.02	0.81	0.24
0.4	A	38.19	-0.3	0.22	1.05	0.19
	B_0	33.19	0.64	0.23	0.88	0.11
	B_1	28.29	0.33	0.26	1.18	0.16
	B_2	16.44	0.21	0.5	0.7	0.13
	B_3	13.45	0.7	0.6	1.12	0.09
	C_A	——	0.88	0.28	1.5	0.08
	C_B	——	0.47	−0.02	0.52	0.24
0.6	A	36.7	0.01	0.21	1.15	0.11
	B_0	32.11	-0.06	0.28	1.98	0.09
	B_1	30.68	0.03	0.31	1.23	0.13
	B_2	21.26	0.05	0.23	1.61	0.14
	B_3	13.98	-0.08	0.27	1.17	0.11
	C_A	—-	1.35	0.2	1.12	0.13
	C_B	—-	0.45	0.21	0.4	0.29
0.8	A	35.51	-0.32	0.13	0.95	0.13
	B_0	32.63	0.21	0.16	0.6	0.08
	B_1	27.23	-0.2	0.14	0.89	0.13
	B_2	20.9	-0.35	0.17	0.84	0.13
	B_3	14.95	-0.4	0.15	0.62	0.08
	C_A	—-	-1.03	0.1	0.96	0.2
	C_B	—-	0.39	0.03	0.45	0.25
1	A	50.73	-0.23	0.31	1.25	0.19
	B	27.65	-0.33	0.39	1.96	0.29
	C_A	——	0.4	0.01	0.44	0.18
	C_B	——	0.6	−0.01	0.67	0.34
Error		±0.2	±0.02	±0.02	±0.02	±0.02

Table 1 indicates that the magnetic field H of the subpatterns B_n decreases with increasing Zn^{2+} ion number n. This clears the dependence of H on the distribution of Zn^{2+} ions among the A-sites as nearest neighbours of the B-site Fe ions. The average reduction of H (ΔH) is about 7 T for x $\leq$ 0.4 and 6 T for x = 0.6 and 0.8. The isomer shift values δ of B_n subpatterns lie between 0.14 and 0.6 mm/s, corresponding to characteristics of the high spin Fe^{3+} charge state [12, 13]. The values of the quadrupole shift ε_Q can provide us information about the electric field gradient EFG inside the samples. The ε_Q values for B_n subpatterns show an increasing trend with increasing number of Zn^{2+} ions. This reveals an increasing deviation from the ideal crystal symmetry [7] as the number of Zn^{2+} ions increases with the A-site nearest neighbors of Fe ions. The δ values for Fe^{3+} at the A-sites lie between 0.13 and 0.31 mm/s and clearly show a decreasing trend corresponding to Cr^{3+} additions. This is consistent with Fe^{3+} ions in spinel ferrites [7, 8]. Consequently, the distribution of S-electron charge of the Fe^{3+} ions is influenced by Cr^{3+} ion substitution. Variations of isomer shifts are due to the difference in the Fe^{3+}-O^{2-} internuclear bond separations at A- and B-sites. The ε_Q value for A-sites is independent on Cr^{3+} concentration and lies between 0.01 and 0.32 mm/s. However, the change of ε_Q may be understood in terms of the deviation of local symmetry from cubic symmetry. The change of sign may originate from the chemical disorder, where this disorder can produces a distribution of EFGs of varying magnitude, direction, sign and asymmetry [12]. It may be due to the deformation of the $3d^5$ shell as a consequence of the trigonal; distortion of the B-site oxygen coordination. The high values of ε_Q and δ reveal the existence of Fe^{2+} ions on the A- and B-sites in these samples. The high values of δ represent a mixed valence state of Fe^{3+} and Fe^{2+} ions. This state is associated with fast electron hopping between neighboring of Fe^{3+} and Fe^{2+} ions [14, 15]. The existence of Fe^{2+} ions on the A- and B-sites is confirmed by IR studies (section 3.2).

The existence of two quadrupole doublets C_A and C_B have been observed previously [16, 17]. Table 1 illustrates that the paramagnetic phase area A_c increases only for $x > 0.4$ with increasing Cr^{3+} concentration x. The doublet structure is due to the quadrupole reaction of ^{57}Fe nuclei located on the A- and B-sites with the electric field gradient (EFG) at those sites. Thus the value of ε_Q can provide information concerning the symmetry of the crystal lattice and its local distortions. For C_A and C_B, the ε_Q absolute values lie between 0.32 and 1.35 mm/sec and change randomly with x. These may result from the random distribution of differently charged cations on the A- and B-sites, which affects EFG, and it may be the consequence of the trigonal distortion of the B-site oxygen coordination, i.e. the deformation of the $3d^5$ shell. Figure 3 illustrates that the area ratio of B- to A-site subspectra increases with x giving a maximum value at x = 0.6, decreasing to the lowest value at $x = 1$ [18]. This behavior is due to the statistics of the cation distribution. It is well known that the Zn^{2+} ions exclusively occupy the A-sites [1–6] and the Cr^{3+} ions the B-sites and the preferred site for the Ni^{2+} ions is the B-sites [6–8]. Consequently the cations distribution can be estimated as given in Table 2, using the site preference of elements and the ratio of area under the well resolved patterns belonging to the A and B sublattices. The increase of Cr^{3+} ions reduces the Fe^{3+} ions at B-sites for $x > 0.6$. From these observations it can be inferred that the Cr^{3+} ions are concentrated at B-sites and the tetrahedral environment of a B-site Fe^{3+} ion remains unchanged noticeably with increasing x. Hence the change of the outermost line width $\Gamma_{1,6}$ at both A- and B-sites is due to the distribution of Zn^{2+} ions and to the change of cations at B-site.

Table 2. Cation distribution in the ferrite system $Ni_{0.5}Zn_{0.5}Cr_xFe_{2-x}O_4$.

X	A-site	B-site
0	$Zn_{0.4}Fe_{0.6}$	$Zn_{0.1}Ni_{0.5}Fe_{1.4}$
0.2	$Zn_{0.48}Fe_{0.52}$	$Zn_{0.02}Ni_{0.5}Cr_{0.2}Fe_{1.28}$
0.4	$Zn_{0.5}Ni_{0.07}Fe_{0.43}$	$Ni_{0.43}Cr_{0.4}Fe_{1.17}$
0.6	$Zn_{0.5}Ni_{0.16}Fe_{0.34}$	$Ni_{0.34}Cr_{0.6}Fe_{1.06}$
0.8	$Zn_{0.5}Ni_{0.1}Fe_{0.4}$	$Ni_{0.4}Cr_{0.8}Fe_{0.8}$
1	$Zn_{0.5}Ni_{0.13}Fe_{0.37}$	$Ni_{0.37}Cr_1Fe_{0.63}$

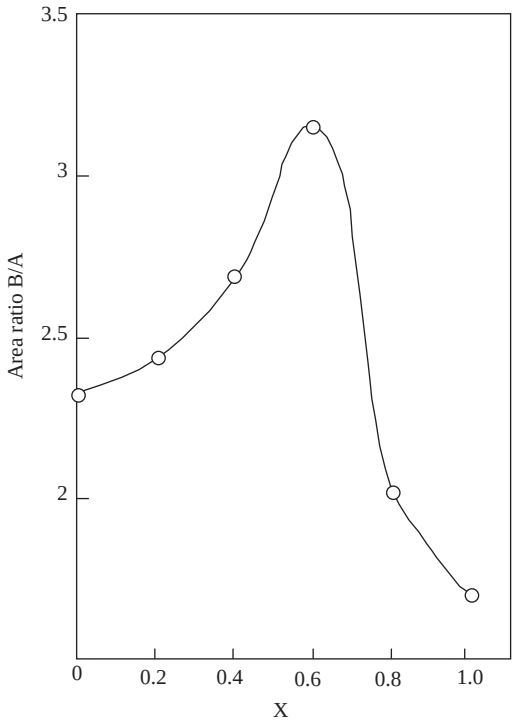

Figure 3. The variation of the area ratio of the B- to A-site subspectra against x.

The behavior of hyperfine magnetic fields at A- sites (H_A) and the average at B-sites (H_B) as functions of Cr^{3+} concentration is shown in Figure 4a. H_A was found to be greater than H_B and decrease for $x \leq 0.8$, whereas H_B decreases only for $x \leq 0.2$. This decrease of H_A and H_B can be understood on the basis of the superexchange interaction and the cations distribution. Though the Neel ordering in most magnetically ordered spinel phases are determined mainly by the strong antiferromagnetic A-B interaction while the contribution of A-A and B-B interactions remain very weak [19], in our cases, it is necessary to take not only the A-B superexchange but also the B-B supertransferred hyperfine interactions into account. In the cations distribution, Zn^{2+} ions are non-magnetic and do not contribute to the nuclear magnetic field. Also, the Fe^{3+}-O^{2-}-Fe^{3+} superexchange interaction is higher than the Fe^{3+}-O^{2-}-Ni^{2+} [20] and than Fe^{3+}-O^{2-}-Cr^{3+} [18, 19]. As a result, H_A and H_B decrease with increasing Cr^{3+} concentration. The sharp increase of H_A at $x = 1$ and H_B at $x \geq 0.4$ may be attributed to a stronger A-B superexchange interaction arising from the presence of a large amount of magnetic ions at B-site. This increase may reflect a ferromagnetic interaction between the magnetic ions within the sublattices. This increment agrees with that observed previously in Cu-Cr ferrite [6]. To explain the behavior of H_A and H_B, the spontaneous magnetization M_s of the bulk material was calculated as was done in [20]. It is known that the average nuclear magnetic field for Fe^{3+} ions in each of the two sublattices is proportional to the average magnetization of the sublattice. Its corresponding area multiplies the hyperfine magnetic field of each sublattice and the difference gives the magnetization M_s of the bulk sample, shown in Figure 4b. The values of M_s increases with x to the maximum value at $x = 0.6$, decreases for $x > 0.6$, and inverted at $x = 1$. The behavior of M_s is similar to that of Zn-ferrites [19, 21].

3.2. Infrared spectra

The most interesting feature of this study is the IR spectra shown in Figure 5. The results of IR studies are listed in Table 3. The two strong absorption bands, ν_1 and ν_2 are observed and assigned to the complexes of Fe^{3+}-O^{2-} at the A-site and of Fe^{3+}-O^{2-} and Cr^{3+}-O^{2-} at the B-site vibrational modes [18, 22–25]. The

change in band positions is due to the change in the Fe^{3+}-O^{2-} internuclear distances for the A- and B-sites. Figure 5 and Table 3 show clearly that the bands ν_1 and ν_2 shift towards the high energy with increasing Cr^{3+}substitution for Fe^{3+} ions. This may be explained on the basis of decreasing the concentration of Fe^{3+} ions amongst the A- and B-sites, which cause increasing the metal-oxygen stretching vibrational energies and cause decreasing the B-site ionic radius and reducing the size of the unit cell i.e. the lattice parameter a (sec. 3.3) [9]. The band ν_3 results from the splitting of the band ν_2 by the increasing presence of the Fe^{2+} ions at the B-site. Thus the band ν_3 can be assigned originally to the Fe^{2+}-O^{2-} complexes and to the divalent metal ion-oxygen complexes in the B-sites [21–25]. The intensity of the band ν_3 increases with increasing Cr^{3+} concentration at B-sites. Accordingly, the increasing existence of Fe^{2+} results from the hopping process between Fe^{3+} and both Ni^{2+} and Cr^{3+} ions as follows [5]:

$$Fe^{3+} + Ni^{2+} \leftrightarrow Fe^{2+} + Ni^{3+}, \; Fe^{3+} + Cr^{3+} \leftrightarrow Fe^{2+} + Cr^{4+}.$$

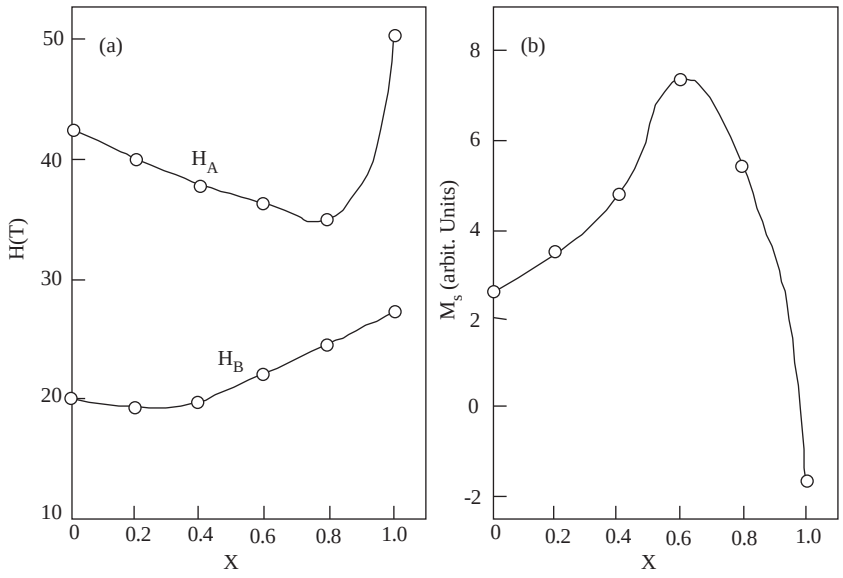

Figure 4. The drawing of (a) the hyperfine magnetic field at the A-site H_A and the B-site (the average) H_B and (b) the calculated spontaneous magnetization Ms, as functions of x.

Table 3. The absorption band positions ν_n and their intensities I_n (n = 0, 1, 2, 3 and SP), SP denotes "splitting" and Sh denotes "Shoulder."

x	ν_{SP} (cm^{-1})	I_{SP}	ν_0 (cm^{-1})	I_0	ν_1 (cm^{-1})	I_1	ν_2 (cm^{-1})	I_2	ν_3 (cm^{-1})	I_3
0	—	—	—	—	577	13	454	14	—	—
0.2	1084–1043	26	Sh	—	548	13	395	17	—	—
0.4	1082–1042	43	881	40	585	14	471	19	344	20
0.6	1082–1043	46	880	32	592	15	484	22	340	27
0.8	1082–1041	28	882	63	562	17	438	24	341	29
1	1082–1040	52	880	82	601	21	496	27	342	33
	±2	±2	±2	±2	±2	±2	±2	±2	±2	±2

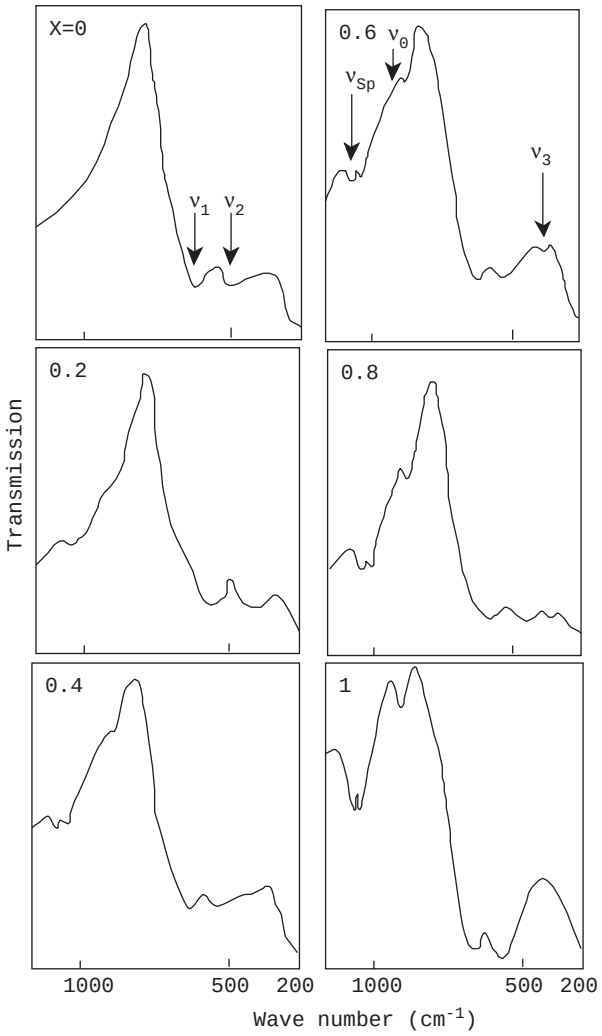

Figure 5. The infrared transmittance spectra for the system $Ni_{0.5}Zn_{0.5}Cr_xFe_{2-x}O_4$.

Whereas Ni^{3+} migrates to the A-sites, the Fe^{2+} and Cr^{4+} remain at the B-sites. Consequently, the number of Fe^{2+} ions increases at B-sites by increasing Cr^{3+} addition. Two bands, ν_o and the splitting band ν_{SP}, appeared around ν_1 and became more pronounced with increasing Cr^{3+} ions content. The band ν_o was observed in the spectra of the Co-Ni ferrites and assigned to the intrinsic vibrations of the tetrahedral group [26, 27]. Some authors [22, 28] reported that the peak ν_o is generally found very intense in the spinel oxides (675 cm^{-1} in Fe_3O_4). They assigned the peak to the breathing mode of the tetrahedral A-sites or to a compound due to the distribution of particle morphologies. Two side bands around ν_1 (600 cm^{-1}) were found in studying Ni-Zn ferrites and assigned these two bands to the presence of Fe^{2+} ions in both A- and B-sites [28]. In the present study, the two bands ν_o and ν_{SP} are clearly dependent on the statistical distribution of the cations amongst the A- and B-sites and on the Cr^{3+} ion concentration at B-site. The splitting band ν_{SP} appeared in studying Co-Zn ferrite [29]. It was assigned to the greater concentration of Fe^{2+} ions and to the distortion of the spinel lattice. In our system, the ν_{SP} band can be assigned to the Cr^{4+}-O^{2-} complexes and to the local distortion of the cubic spinel lattice [28, 29]. The ν_o band may be due to increasing the concentration of the Fe^{2+} and Ni^{2+} ions at A-sites [26].

Actually, the bands ν_o and ν_{SP} result from the splitting of the band ν_1 and ν_3 from the splitting of ν_2. These splits are characteristic of the Jahn-Teller effect of the ions Fe^{2+}, Ni^{2+} and/or Cr^{4+} at A- and B-sites [26], where the Jahn-Teller effect can cause a local distortion of the cubic spinel lattice [26]. The intensity of

the band ν_{SP} increases with increasing chromium addition. This reveals increasing the number of the Cr^{4+} ions at the B-sites by the hopping process.

The refractive index R and the velocity V of the IR waves in the samples can be estimated at the band ν_1 using the relation [23, 30]:

$$\frac{E_t}{E_{ab}} = \frac{c}{V} = R,$$

where E_t is the transmitted energy, E_{ab} the absorbed energy and c is the velocity of light. The obtained values of R and V, as shown in Figure 6a, indicate that the refractive index decreases, whereas the velocity of IR increases against x. The jump rate J of the lattice vacancies may be estimated from the relation [23, 30]: $J = \nu e^{E/kT}$, where $\nu$is the frequency of the vibration, k is the Boltzmann constant, $E = h\nu = {}^{V}/_{\lambda}$, h is Plank's constant and λ is the IR wavelength. Figure 6b illustrates that the jump rate J of the lattice vacancies increases with increasing Cr^{3+} concentration x. The increase of the absorbed energy at ν_1 leads to decreasing the refractive index R with x. The substitution process x increases the Fe_A^{3+}- O^{2-} bond length d_{AL} (see sec. 3.3 below), and weakens the B-B superexchange interactions. This leads to vibrating the lattice at high frequency with the incident IR waves and to increasing the IR wave velocity V inside the samples. Increasing the jump rate J is attributed to increasing the cation vacancies by the formation of the larger ions Fe^{2+} (0.76 Å) by the hopping process in the lattice. The formation of larger ions increases the lattice vacancies and increases the jump rate [31].

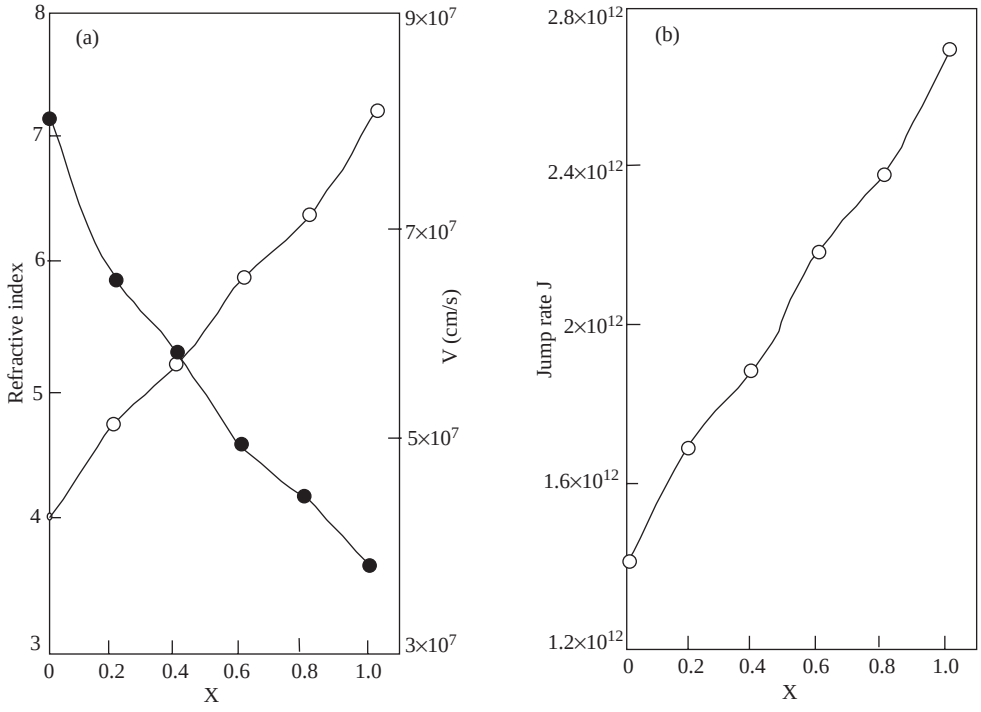

Figure 6. The effect of the Cr^{3+} concentration x on (a) the IR refractive index R and velocity V ,and (b) the jump rate of the cationic vacancies.

3.3. X-ray analysis

The deduced parameters from the X-ray diffraction patterns, shown in Figure 1, are given in Table 4. The values of the lattice parameter a for all samples lie between 8.359 and 8.579 Å, and of the interplanar distance d between 1.275 and 3.025 Å, which agree with that obtained previously [6, 9, 32], and ASTM cards.

Table 4. The calculated X-ray parameters; the tetrahedral and octahedral bond length, d_{AL} and d_{BL}, and hopping length, L_A and L_B, the tetrahedral edge d_{AE}, the shared and unshared octahedral edge d_{BE} and d_{BEU}, and the true and theoretical lattice parameters a_t and a_{th}.

X	d_{AL} (Å)	d_{BL}(Å)	d_{AE} (Å)	d_{BE} (Å)	d_{BEU}(Å)	a_t (Å)	a_{th} (Å)	L_A(Å)	L_B(Å)
0	2.095	1.952	3.421	2.518	2.986	8.4	8.4	3.667	3.006
0.2	2.118	1.939	3.458	2.476	2.987	8.394	8.389	3.642	2.974
0.4	2.147	1.925	3.505	2.428	2.991	8.382	8.378	3.634	2.968
0.6	2.15	1.922	3.51	2.412	2.9904	8.394	8.379	3.631	2.965
0.8	2.154	1.92	3.517	2.418	2.9905	8.368	8.3661	3.623	2.958
1	2.144	1.9	3.492	2.379	2.992	8.334	8.35	3.596	2.936

The variation of both the average lattice parameter a_o and the theoretical density D_x versus the chromium concentration x is shown in Figure 7a. It is shown that a_o and D_x decrease slightly and linearly with x. The decrement of a_o is assigned to the substitution of the smaller radius Cr^{3+} ion (0.64 Å) for Fe^{3+} ion (0.67 Å). The relation between both the bulk density D and porosity P and x is illustrated in Figure 7b. Here, we see that D decreases, whereas p increases with x. The increase of P may be due to the reduction of oxygen vacancies, which play a predominant role in accelerating densification [32]. The decrement of D_x and D may be attributed to the lighter atomic weight of Cr^{3+} ion (51.996) as compared to that of Fe^{3+} ion (55.847). A plot of the measured lattice parameter a, versus the Nelson-Riley function [33, 34]

$$F(\theta) = \frac{1}{2}\left(\frac{\cos^2\theta}{\sin\theta} + \frac{\cos^2\theta}{\theta}\right),$$

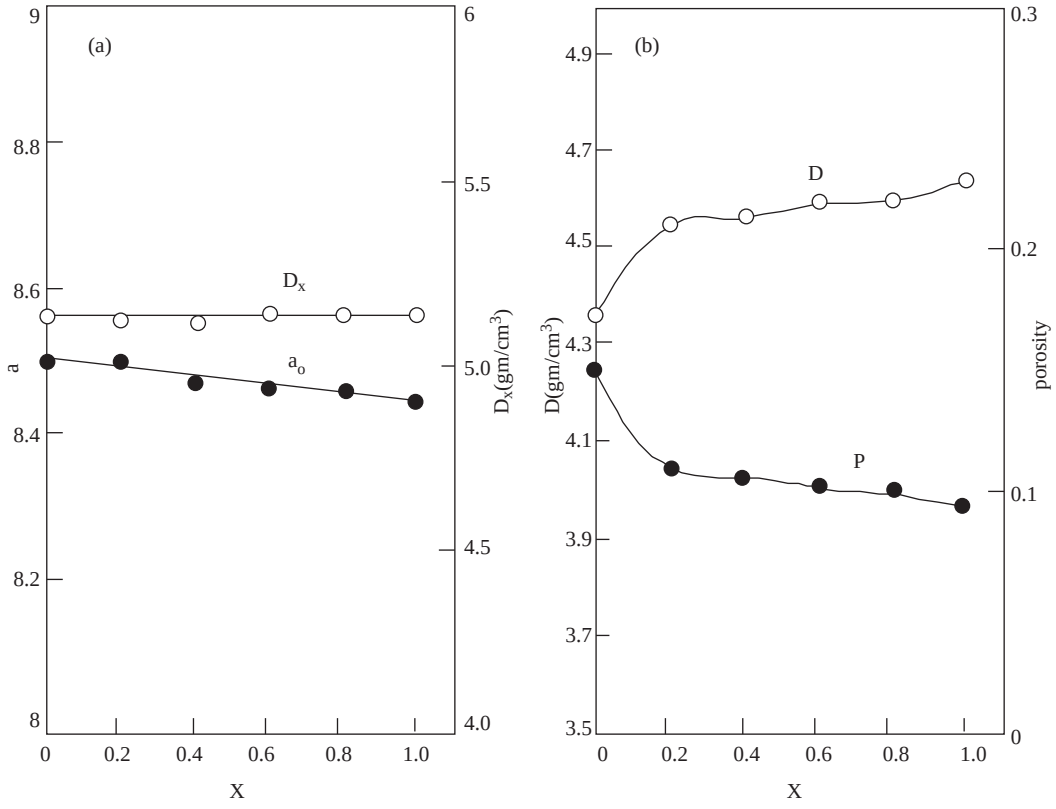

Figure 7. The variation of (a) the average lattice parameter a_o and the bulk density D_x , and (b) the theoretical density D and the porosity P, against x.

is shown in Figure 8. The plots are straight lines with increasing trend. The true lattice parameter a_t can be obtained by extrapolating the lines to F (θ)= 0 at $\theta = 90°$. The obtained values of a_t are listed in Table 4. The deduced cations distribution may be confirmed by using it for calculating the theoretical lattice parameter a_{th} as follows [35]:

$$a_{th} = \frac{8}{3\sqrt{3}}(r_A + r_0) + \sqrt{3}(r_B + r_0)$$

where r_A is the mean site ionic radius of the A-site, r_B of the B-site and r_0 is the radius of the oxygen ion O^{2-} (1.48 Å). The calculated values of a_{th} are given in Table 4. The comparison between the obtained values for both a_t and a_{th} illustrates that their values are approximately equal, which confirm the estimated cations distribution. The oxygen parameter u can be obtained from the relation [15, 35–38];

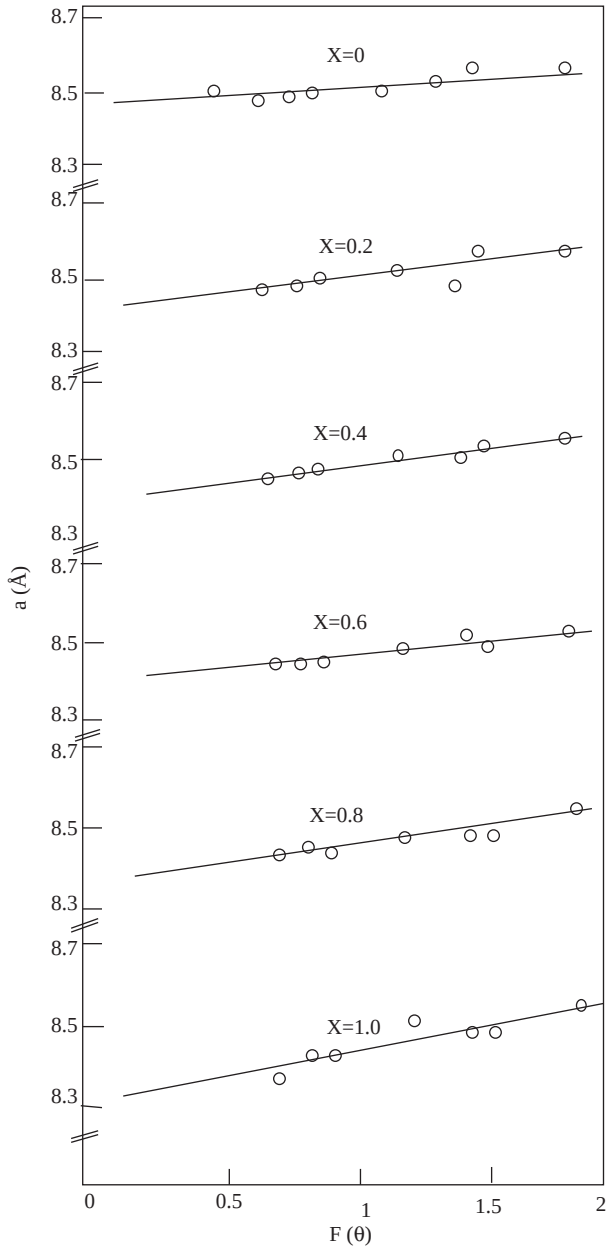

Figure 8. The relation between Nelson-Riley F(θ) and the lattice parameters a.

$$r_A = a_t\sqrt{3}(u - \frac{1}{4}) - r_o$$

The mean ionic radius of the A-site r_A may be calculated as [14, 35–39]

$$r_A = (z)r^{3+}_{tet.Fe} + (0.5 - z)r^{2+}_{tet.Ni} + (0.5)r^{2+}_{tet.Zn},$$

where z denotes the concentration of Fe^{3+} ions at the A-sites. Consequently, the mean ionic radius of the B-site molecule r_B may be calculated from the equation

$$r_b = [2 - (x + z)]r^{3+}_{oct\,Fe} + (x)r^{3+}_{oct\,Cr} + (z)r^{2+}_{oct\,Ni}$$

The relation between u, r_A and r_B and x is shown in Figure 9a. It is clear that r_B decreases noticeably as a function of x, whereas u and r_A increase slowly. This observation may be due to the correlation between the ionic radius and the lattice parameters [28, 38]. The decrease of r_B is due to the replacement of the Fe^{3+} ions at the octahedral B-sites by the smaller radius Cr^{3+} ions. The increase of r_A may be due to the increasingly migration of the larger Ni^{2+} (0.72 Å) and Zn^{2+} (0.82 Å) ions to the A-sites instead of Fe^{3+} ions, as indicated in Table 2. The increase of u is a direct consequence of increasing the trigonal distortion of the B-site oxygen coordination. Increasing the migration of the ions Ni^{2+} and Zn^{2+} into the A-sublattice makes it expand to accommodate these ions. This expansion creates oxygen vacancies in the A-sites, which increases the trigonal distortion of the B-site oxygen coordination. This is reflected in the obtained high values of u (0.4), where the ideal value is 0.375.

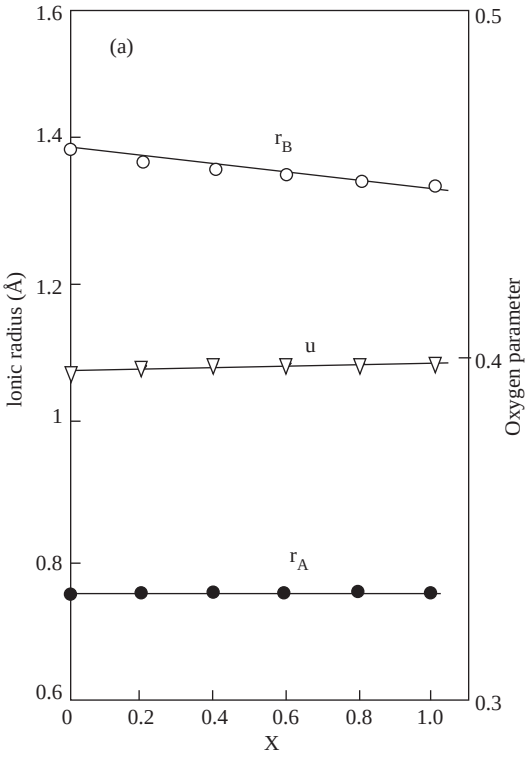

Figure 9. The behaviour of the ionic radius of the A-site r_A and of the B-site r_B and the oxygen positional parameter u as functions of x.

Using the values of a_t and u the tetrahedral and octahedral bond length, d_{AL} and d_{BL}, the tetrahedral edge d_{AE} and the shared and unshared octahedral edge, d_{BE} and d_{BEU}, may be calculated as follows [35–38]:

$d_{AL} = a_t\sqrt{3}\left(u - \frac{1}{4}\right)$ tet. bond.
$d_{BL} = a_t\left(3u^2 - \frac{11}{4}u + \frac{43}{64}\right)^{\frac{1}{2}}$ oct. bond.
$d_{AE} = a_t\sqrt{2}\left(2u - \frac{1}{2}\right)$ tet. edge
$d_{BE} = a_t\sqrt{2}(1 - 2u)$ shared oct. edge.
$d_{BEU} = a_t\left(4u^2 - 3u + \frac{11}{16}\right)^{\frac{1}{2}}$ unshared oct. edge.

The calculated values are listed in Table 4. While d_{AL}, d_{AE} and d_{BEU} increase with x, d_{BL} and d_{BE} decrease. The decrease of d_{BL} and d_{BE} is attributed to the smaller radius of the added Cr^{3+} ions into the B-sites as compared with the substituted Fe^{3+} ions. The increase of d_{AL}, d_{AE} and d_{BEU} may be due to the migration of the larger Ni^{2+} and Zn^{2+} ions into the A-sites.

3.4. The effect of the hopping lengths on the hyperfine magnetic fields

The distance between the magnetic ions (the hopping length) L is given by $L_A = a_0\sqrt{3}/4$ for the A-sites and by $L_B = a_0\sqrt{2}/4$ for the B-sites [37, 38]. The obtained values of L_A and L_B are listed in Table 4. It is clear that both L_A and L_B decrease with increasing x. This is attributed to the substitution process and the reduction of the size of the unit cell (a_o). The migrating of the magnetic ions Ni^{2+} into the A-sublattices and the introducing the Cr^{3+} ions into the B-sublattices make the magnetic ions approach to each other and decrease the hopping length between them.

The dependence of the magnetic fields H_A and H_B on the hopping lengths L_A and L_B [39], respectively, is shown in Figure 10. It is shown that H_A and H_B reflect the same behavior with increasing L. Their highest values are at the least distance between the ions, where they decrease sharply to a minimum value for each. This minimum value depends on the distance L at the corresponding site. However, Increasing the distance L between the site-ions slow increases the hyperfine field at this site. This may be explained as follows; (1) it is known that the ions Ni^{3+} and Cr^{4+} are nonmagnetic, the magnetic moment of Fe^{2+} ion is less than that of Fe^{3+} ion and the hopping process between the magnetic cations produces Ni^{3+}, Cr^{4+} and Fe^{2+} ions. (2) Introducing a highest concentration of the smaller Cr^{3+} ions (the least L) into the B-sublattices creates a cation vacancies, which can block the hopping process between Fe^{3+} and Ni^{2+}, (3) The high content of Cr^{3+} can activate the hopping process between Cr^{3+} and both Ni^{3+} and Fe^{2+} transforming them to Ni^{2+} and Fe^{3+} ions and giving rise the highest magnetic fields of the sublattices, (4) Hence, decreasing the Cr^{3+} concentrations (increasing L) increases the hopping process between Fe^{3+} and Ni^{2+}, therefore H_A and H_B decrease to a critical value, (5) above this value the concentration of Fe^{3+} ions increase instead of Cr^{3+} ions i. e. the number of the magnetic bonds Fe^{3+}- O^{2-} - Fe^{3+} increase and then H_A and H_B increase.

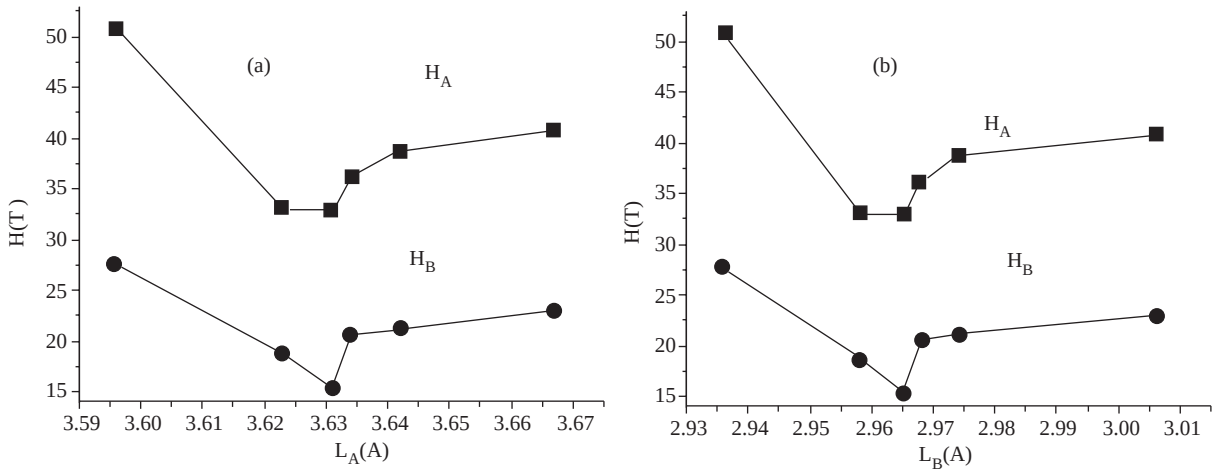

Figure 10. The dependence of the hyperfine fields H_A and H_B on the distance between the magnetic ions at the A-sites L_A (a), and B-sites L_B (b), respectively.

4. Conclusion

IR and X-ray studies have demonstrated the spinel structure of the studied system. The Mössbauer spectra of the system consist of a broad six-line magnetic pattern and a central paramagnetic phase. The spectra have been fitted to two magnetic subpatterns A and B and two quadrupole doublets C_A and C_B. Patterns A and C_A are attributed to F^{3+} ions at the tetrahedral A-sites and B and C_B are attributed to F^{3+} and Fe^{2+} ions at the octahedral B-sites. The isomer shift, quadrupole shift, line width and quadrupole doublet splitting were change randomly with increasing the Cr^{3+} concentration. The paramagnetic phase area, the area ratio of the B- to A-sites, the hyperfine magnetic field at A- and B-sites, H_A and H_B, and the magnetization depended on Cr^{3+} content. The cation distribution has been estimated and confirmed by X-ray study. The composite B patterns belonging to the B-site has been analyzed to its multicomponents, depending on the distribution of the Zn^{2+} ions as nearest neighbors of the A-site. Mössbauer studies reveal the existence of Fe^{2+} ions at the A- and B-sites. Five IR absorption bands are reported in the range from 1100 to 200 cm^{-1}. They confirm the presence of Fe^{2+} ions at the A- and B-sites, formed by the hopping process between Fe^{3+} and both Ni^{2+} and Cr^{3+} ions. The calculated hopping length between the magnetic ions was found to decrease with x, where the magnetic fields H_A and H_B showed a hopping length- dependence. The additions of Cr^{3+} ions change the band positions and shift the bands ν_1 and ν_2 towards the high-energy side. The velocity of the IR waves and the jump rate of the lattice vacancies were found to increase, whereas the IR refractive index decreases against x. From X-ray studies, the calculated parameters were found to be dependent on the Cr^{3+} content. The porosity, the A-site ionic radius, bond length and edge and the oxygen positional parameter were increasing with increasing x, whereas B-site radius, bond length, shared and unshared edge, the bulk and theoretical density, and the lattice parameter were decreasing. This variation is assigned to the substitution process and the migration of the Ni^{2+} and Zn^{2+} ions into the A-sites.

References

[1] N. Rezlescu, E. Rezlescu, C. Pasnicu and M. L. Craus, *J. Phys. Condens. Matter.*, **6**, 1994), 5707.

[2] C. Sung, W. C. Ki, S. Y. An and S. . Lee, *J. Magn. Magn. Mater.*, **215–216**, (2000), 213.

[3] Yu G. Chukalkin and V. R. Shtirts, *Phys. Stat. Sol. (a)*, **160**, (1997), 185.

[4] J. Waerenborgh, M. Figuered, J. M.Cabrol and L. Pereiro, *J. Solid State Chem.*, **111**, (1994), 300.

[5] A. K. Singh, T. C. Goel and R. G. Mendiratta, *J. Magn. Magn. Mater.*, **125/2**, (2003), 121.

[6] M. A. Amer, M. A. Ahmed, M. K. El-Nimr and M. K. Mustafa, *Hyperfine Interact.,* **96**, (1995), 91.

[7] A. M. Sankpal, S. Suryavanshi, S. Kakatkar, G. Tengshe, R. Patil, N. Chaudhari and S. Sawant, *J. Mag. Mag. Mater.*, **186/3**, (1998), 349.

[8] H. N. Ok, K. S. Baek and E. J. Chsi, *Phys. Rev. B,* **40**, (1989), 84.

[9] M. A. Amer, *Phys. Stat. Sol. (a),* **151**, (1995), 205.

[10] E. De Grave, R. Van Leerberghe, C. Dauwe, J. De Sitter and A. Covaert, *J. Phys. Collog.*, **37/C6**, (1976), 97.

[11] E. De Grave, A. Covaert, D. Chambaere and C. Robbrecht, , *J. Phys. Collog.*, **40/C2**, (1979), 669.

[12] H. N. Ok and B. J. Evans, *Phys. Rev. B,* **14**, (1976), 2956.

[13] H. N. Ok, K. S. Baek, H. S. Lee and C. S. Kim, *Phys. Rev. B*, **41**, (1990), 62.

[14] M. A. Amer, *Phs. Stat. Sol. (a)*, **181**, (2000), 539.

[15] M. A. Amer and O. M. Hemeda, *Hyperfine Interactions,* **96**, (1995), 99.

[16] R. Van Leerberghe and R. E. Vandenberghe, *Hyperfine Interactions*, **23**, (1985), 75.

[17] R. Gerardin, A. Randani, C. Gleitzer, B. Gillot and B. Durand, *J. Solid State Chem.*, **57**, (1985), 215.

[18] L. K. Leung, B. J. Evans and R. Renaudin, *Phys. Rev. B*, (1973), 29.

[19] J. S. Baijal, D. Kothari, S. Phanjoubam and C. Prakash, *Solid state commun.*, **69**, (1989), 277.

[20] D. C. Dobson, J.W. Linnet and M. M. Rahman, *J. Phys. Chem Solids,* **31**, (1970), 2727.

[21] M. A. Amer, *Phys. Stat. Sol. (a),* **145**, (1994), 157.

[22] M. I. Baraton, V. Lorenzelli, G. Busca and R.Jj. Willy, *J. Mater. Sci. Letters*, **13**, (1994), 275.

[23] O. M. Hemeda, *J. Mag. and Mag. Mater.*, **281**, (2004), 36.

[24] D. Ravinder and V. Kumar, *Bull. Mater. Sci.*, **24**, (2001), 505.

[25] O. M. Hemeda and M. I. Abd EL-Ati, *J. Mag. Mag. Mater.*, **51**, (2001), 42.

[26] S. A. Patil, S. M. Otari, V. C. Mahajan, M. G. Patil, A. B. Patil, M. K. Soudajar, B. L. Patil and S. R. Sawant, *Solid State Comm.*, **78/1**, (1991), 39.

[27] M. K. El-Nimr, M. A. Ahmed and M. A. El hiti, *J. Mater. Sci. Letters,* **13**, (1994),1500.

[28] V. A. Potokova, N. D. Zverv and V. P. Romanov, *Phys Stat. Sol. (a)*, **12**, (1972), 623.

[29] N. Z. Darwish, *Appl. Phys. Commun.*, **13**, (1994), 243.

[30] J. Neumann, M. O. Rowe, H. Veenhuis, R. Pankrath and E. Kratzig, *Phys. Stat. Sol. (b),* **215**, (1999), R9.

[31] O. M. Hemeda and M. M. Barakat, *J. Mag. Mag. Mater.*, **323**, (2001), 127.

[32] J. B. Nelson and D. P. riley, *Proc. Phys. Soc., London*, **57**, (1945), 160.

[33] O. M. Hemeda, M. A. Amer, S. Aboul-Enein and M. Ahmed, *Phys. Stat. Sol. (a),* **156**, (1996), 29.

[34] A. A. Yousif, M. E. Elzain, S. A. mazen, H. H. Sutherland, M. h. Abd-allah and S. F. Mansour, *J. Phys. Condens. Matter,* **6**, (1994), 5717.

[35] O. Ravinder, *J. Appl. Phys.*, **75**, (1994), 6121.

[36] C. Arean, J. Blanco, J. Gonzales and M. Fernandez, *J. Matter. Sci. Lett.*, **9**, (1990), 229.

[37] P. V. Reddy and T. Seshegirirao, *J. Less-Common Metals,* **75**, (1980), 255.

[38] H. Pascard, A. Globus and V. Cabon, *J. Physique,* **38 C1**, (1977), 163.

[39] M. El-Saadawy and M. Barakat, *J. Mag. Mag. Mat.*, **213**, (2000), 309.